

Investigation of negative photoconductivity in p-type $\text{Pb}_{1-x}\text{Sn}_x\text{Te}$ film

M. A. B. Tavares, M. J. da Silva, M. L. Peres, S. de Castro, D. A. W. Soares, A. K. Okazaki, C. I. Fornari, P. H. O. Rappl, and E. Abramof

Citation: *Appl. Phys. Lett.* **110**, 042102 (2017); doi: 10.1063/1.4974539

View online: <http://dx.doi.org/10.1063/1.4974539>

View Table of Contents: <http://aip.scitation.org/toc/apl/110/4>

Published by the [American Institute of Physics](#)

Articles you may be interested in

[The role of bandgap energy excess in surface emission of terahertz radiation from semiconductors](#)

Appl. Phys. Lett. **110**, 042101042101 (2017); 10.1063/1.4974479

[Electrical properties of Si-doped GaN prepared using pulsed sputtering](#)

Appl. Phys. Lett. **110**, 042103042103 (2017); 10.1063/1.4975056

[Optical generation of pure spin currents at the indirect gap of bulk Si](#)

Appl. Phys. Lett. **110**, 042403042403 (2017); 10.1063/1.4974820

[Mid-IR colloidal quantum dot detectors enhanced by optical nano-antennas](#)

Appl. Phys. Lett. **110**, 041106041106 (2017); 10.1063/1.4975058



Small Conferences. BIG Ideas.

Applied Physics Reviews

SAVE THE DATE!

3D Bioprinting: Physical and Chemical Processes

May 2–3, 2017 • Winston Salem, NC, USA

Investigation of negative photoconductivity in p -type $\text{Pb}_{1-x}\text{Sn}_x\text{Te}$ film

M. A. B. Tavares,¹ M. J. da Silva,¹ M. L. Peres,¹ S. de Castro,² D. A. W. Soares,¹
 A. K. Okazaki,³ C. I. Fornari,³ P. H. O. Rappl,³ and E. Abramof³

¹Instituto de Física e Química, Universidade Federal de Itajubá, Itajubá, MG CEP 37500-903, Brazil

²Departamento de Física, Universidade Federal de São Carlos, São Carlos – SP 13565-905, Brazil

³Laboratório Associado de Sensores e Materiais, Instituto Nacional de Pesquisas Espaciais, São José dos Campos, PB 515, SP CEP 12201-970, Brazil

(Received 25 October 2016; accepted 10 January 2017; published online 23 January 2017)

We investigated the negative photoconductivity (NPC) effect that was observed in a p -type $\text{Pb}_{1-x}\text{Sn}_x\text{Te}$ film for temperatures varying from 300 K down to 85 K. We found that this effect is a consequence of defect states located in the bandgap which act as trapping levels, changing the relation between generation and recombination rates. Theoretical calculations predict contributions to the NPC from both conduction and valence bands, which are in accordance with the experimental observations. *Published by AIP Publishing.* [<http://dx.doi.org/10.1063/1.4974539>]

PbTe compounds have been used for the development of infrared photodetectors and diode lasers^{1,2} over the decades. In addition to the technological applications, PbTe based structures are much suitable for research in basic physics, i.e., it was verified that there existed strong spin-orbit coupling in films and nanostructures, which indicates that such materials are good candidates for spintronic devices.³ Introduction of Sn atoms makes this material even more interesting for practical applications as well as from the basic physics point of view. According to the band inversion model,⁴ the gap of $\text{Pb}_{1-x}\text{Sn}_x\text{Te}$ decreases as Sn composition increases and vanishes for an intermediate alloy composition. Further increase in Sn concentration leads to the band inversion, and the energy gap starts to increase up to the SnTe value. The temperature at which band inversion occurs depends on the Sn content. For example, for $x \sim 0.44$, the bands are inverted at ~ 60 K. Very recently, it was discovered that in the region of band inversion, transition from metallic to crystalline topological insulator (TCI) occurs.⁵ Hence, after the transition, the system presents a different condensed matter phase, and a series of phenomenon can be investigated. Regarding the phenomenon of photoconductivity, it has been investigated thoroughly in $\text{Pb}_{1-x}\text{Sn}_x\text{Te}$ films and can be found in the literature.^{6,7} Despite the fact that photoconductivity measurements are being performed in several narrow-gap semiconductor materials over the years,^{8–11} the negative photoconductivity (NPC) effect, when the material becomes less conductive in the presence of light, has attracted attention due to its potential application in photodetectors and nonvolatile memories.¹² In fact, the search for such phenomenon at room temperature being the main goal of research groups, several materials are investigated nowadays with potential practical application. Concerning photovoltaic devices fabrication, crystalline and photoconductivity samples with low electrical resistivity are desirable, which make $\text{Pb}_{1-x}\text{Sn}_x\text{Te}$ films good candidates for this purpose, i.e., the electrical resistivity of samples investigated in this work is $2.5 \times 10^{-1} \Omega \text{cm}$ at room temperature and $\sim 5.0 \times 10^{-2} \Omega \text{cm}$ at 77 K. Among the most recent investigated materials that exhibit the NPC effect, the most popular materials are: MoS_2 monolayers,¹³ In_2Se_3 films,¹⁴ Silk protein hydrogels,¹⁵ films of functionalized metal

nanoparticles,¹⁶ and antimony sulfoiodide (SbSI) nanowires,¹⁷ just to cite a few examples. For most of these materials, the NPC effect is a consequence of trap levels inside the bandgap.

For PbTe based materials, it is well known that trap states are located in the bandgap and are originated from the intrinsic disorder introduced during the sample growth.¹⁸ When illuminated, these materials present positive photoconductivity.¹⁹ The introduction of Sn atoms changes the position of the trap level in relation to the maximum of the valence band and alters the generation and recombination rates when the sample is illuminated.¹⁸

In this work, we present the results of photoconductivity measurements performed in p -type $\text{Pb}_{1-x}\text{Sn}_x\text{Te}$ film, grown on the (111) cleaved BaF_2 substrate, for $x \sim 0.44$. We observed that the NPC effect at room temperature with its amplitude increases as the temperature decreases. We show that the NPC effect is a consequence of the reduction of electrons and holes in the conduction and valence bands, respectively, due to the influence of the trap level in the dynamics of the generation and recombination rates when the sample is illuminated.²⁰

The $\text{Pb}_{1-x}\text{Sn}_x\text{Te}$ film was grown in the Riber 32PMBE system equipped with metal rich lead telluride, stoichiometric tin telluride alloys, and two tellurium additional cells to adjust the electrical properties of the film with the deviation from stoichiometry. The beam equivalent pressure (BEP) of each cell is measured before and after growth by the Bayer-Alpert ion gauge placed at the substrate position. The background pressure was 10^{-9} Torr during BEP measurements. The composition of the $\text{Pb}_{1-x}\text{Sn}_x\text{Te}$ layers is determined by the ratio between the BEPs of PbTe and SnTe: $x = \text{BEP}^{(\text{SnTe})} / \text{BEP}^{(\text{PbTe})} + \text{BEP}^{(\text{SnTe})}$. The total thickness of the layer investigated here was $1 \mu\text{m}$. The lattice constant of the $\text{Pb}_{1-x}\text{Sn}_x\text{Te}$ layer was obtained by measuring $a\omega/2\theta$ scan around the (222) x -ray diffraction peaks of film and substrate. Using the BaF_2 Bragg peak as a reference, a lattice parameter of 6.402 \AA was determined from the angular separation between the $\text{Pb}_{1-x}\text{Sn}_x\text{Te}$ and the BaF_2 peaks. Considering Vegard's law and the values of 6.462 \AA and 6.327 \AA for the lattice parameter of PbTe and SnTe,

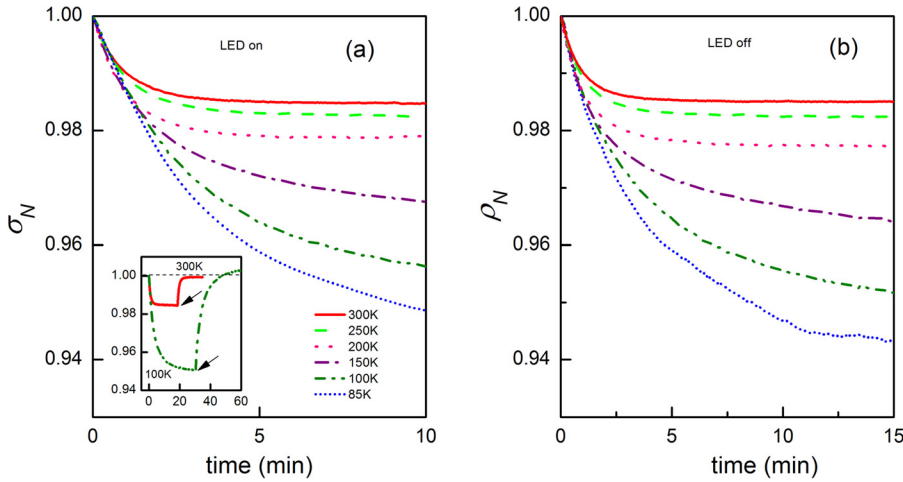


FIG. 1. (a) Time dependence of the normalized photoconductivity ($\sigma_N = \frac{\sigma_{light}}{\sigma_{dark}}$) for the $\text{Pb}_{0.6}\text{Sn}_{0.44}\text{Te}$ film in the temperature range of 85–300 K under illumination. The inset exhibits the buildup and decay at 300 K and 100 K, under illumination and dark conditions (see the arrows for LED off). (b) The values of $\rho_N = 1/\sigma_N$ for the temperatures presented in (a) when the illumination is removed, revealing the effect of persistent photoconductivity.

respectively, the atomic composition of the $\text{Pb}_{1-x}\text{Sn}_x\text{Te}$ layer was determined to be $x=0.44$, the same value as obtained from the BEPs relation. The full-width at half-maximum of the $\text{Pb}_{1-x}\text{Sn}_x\text{Te}(222)$ Bragg peak was 330 arc sec, which indicates the good crystalline quality of the grown layer. Therefore, we have precise control on the growth of single crystal films of PbTe, SnTe, and its pseudo-binary alloys, $\text{Pb}_{1-x}\text{Sn}_x\text{Te}$, since these two compounds are completely soluble in each other. That is, to say, the compound $\text{Pb}_{1-x}\text{Sn}_x\text{Te}$ is a substitutional solid solution with complete solubility and obeys Vegard's law. Pb and Te vacancies in PbTe crystal lattice produce acceptor or donor levels, respectively, with zero activation energy. Therefore, it is possible, by means of extra supply Te BEP, to grow undoped intrinsic films, controlling both the density and the type of charge carriers.²¹

The p -type $\text{Pb}_{1-x}\text{Sn}_x\text{Te}$ film was grown on freshly cleaved (111) BaF_2 substrates (from Korth Kristalle GmbH), pre-heated to 300 °C for 10 min before starting the growth. The film growth was monitored *in situ* by 35 keV reflection high-energy electron diffraction, RHEED, system from Staib Instruments, Inc. As expected, the RHEED diffraction patterns show that $\text{Pb}_{1-x}\text{Sn}_x\text{Te}$ films grow in the layer-by-layer mode, independent of the alloy composition. The growth starts with nucleating islands and, after the coalescence of the islands, it changes to the layer-by-layer mode,²¹ and 2703 monolayers were grown (1 monolayer = 3.7 Å).

The electrical properties of the samples were characterized by resistivity and Hall effect measurements to determine the type and concentration of the majority carriers and their mobility. Such measurements were performed using an automated Keithley 180 A Hall effect system with magnetic fields up to 1.0 T in a temperature range between 77 and 300 K. The electric contact preparation follows the van der Pauw geometry, using gold (Au) wires soldered with indium (In) contacts. For photoconductivity measurements, a blue LED was used with the wavelength of 460 nm and with the intensity of 276 $\mu\text{W}/\text{m}^2$.

Figure 1(a) shows the time dependence of the normalized photoconductivity ($\sigma_N = \frac{\sigma_{light}}{\sigma_{dark}}$) for the $\text{Pb}_{0.6}\text{Sn}_{0.44}\text{Te}$ film in the temperature range of 85–300 K under illumination. According to this figure, the sample presents a clear NPC effect in the whole range of temperatures measured. In addition, the NPC amplitude increases with the decreasing

temperature. The inset in Figure 1(a) exhibits the buildup and decay at 300 K and 100 K, for illumination and dark conditions (see the arrows for LED off). From this inset, it is also possible to observe that the conductivity does not re-establish back to the original value at low temperatures but reaches a higher value instead. Figure 1(b) presents the values of $\rho_N (= 1/\sigma_N)$ for the temperatures presented in Figure 1(a) when the illumination is removed, revealing the effect of persistent photoconductivity, which is expected in PbTe based compounds.¹⁹ This figure also shows that the time decay scales with temperature, indicating the presence of trapping mechanism, which becomes more effective when temperature decreases. Trap levels, in this case, are associated with the disorder present in the system.

In order to investigate the origin of NPC and its temperature dependence observed in this film, we calculated the recombination times, τ , from the decay curves presented in Figure 1(b) using the relation $\sigma(t) = \sigma_0 \exp(-t/\tau)$,⁹ where σ_0 is the electrical conductivity in dark conditions. The values of $\ln(\tau)$ are presented as a function of $1/k_B T$ in Figure 2(a). From a linear fitting, one can extract the ionization energy (or the trap depth) ΔE using the expression⁹

$$\frac{1}{\tau} = \alpha \exp\left(-\frac{\Delta E}{k_B T}\right), \quad (1)$$

where α is a parameter that depends of the density of states and k_B is the Boltzmann constant. The value obtained is

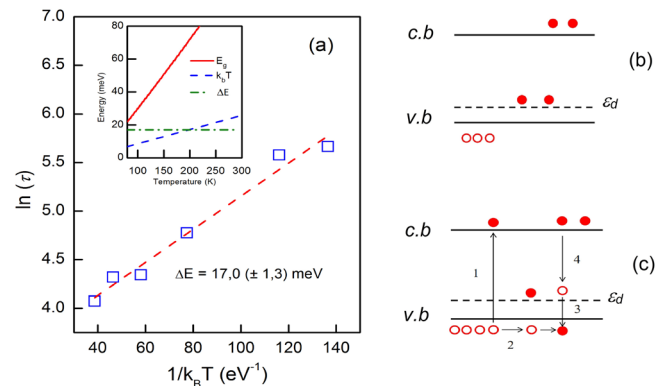


FIG. 2. (a) $\ln(\tau)$ as a function of $1/k_B T$. Inset: Thermal energy $k_B T$, ΔE the energy gap E_g . (b) and (c) schematic representation of the transitions taking in account the trap level (ϵ_d). Dark conditions (b) and under illumination (c).

$\Delta E \sim 17$ meV and corresponds to the energy height of the traps located above the maximum of the valence band. As mentioned before, this level is originated from defect states and has an acceptor character.¹⁸ Undoped PbTe samples contain significant concentrations of lattice point defects like vacancies and interstitials, which produce deviations from the stoichiometric composition.²⁰ It is important to point out that the energy gap in this material decreases as temperatures decreases, which influences the generation and recombination rates of the carriers. The position of the defect level does not change considerably as temperature decreases since there is no variation of the slope of the curve obtained in Figure 2(a). In addition, our computational simulations showed that even considering an overestimated variation of 30% on the defect position, the variation in the generation and recombination rates is negligible.

In order to compare the thermal energy $k_B T$ and ΔE in relation to the position of the energy gap, i.e., the position of the conduction band minimum with respect to the valence band maximum, we plot these energy values in the inset of Figure 2(a), using the following equation to calculate the energy gap in eV:²²

$$E_g(x, T) = 0.19 - 0.543x + 4.5 \times 10^{-4} \frac{T^2}{(T + 50)}. \quad (2)$$

Through the inset, one observes that ΔE becomes close to E_g for temperatures below 150 K. In fact, for $T \sim 70$ K, the system is close to the band inversion, where the transition from metallic to crystalline topological insulator occurs. In this regime, carriers cannot be described by the model since they become Dirac particles. At this situation, when defect level is close to the conduction band minimum, it is not possible to predict the values of generation and recombination rates using classical models. The thermal energy, $k_B T$, is the same order of the ΔE below 200 K, which suggests that around this temperature, trapping mechanism would be more effective; in fact, this is observed and will be explained later.

Hence, for a more realistic analysis of the observed phenomenon, we analyze the data for temperatures higher than 70 K.

The total variation of electrical conductivity is the contribution of the individual variations in valence and conduction bands due to the generation of electron-hole pairs under illumination

$$\Delta\sigma = e(\mu_n \Delta n + \mu_p \Delta p), \quad (3)$$

where μ_n and μ_p are the electrons and holes mobility and Δn and Δp are the density of excess electrons and holes due to illumination. In the absence of trap levels, the generated holes in the valence band correspond to promoted electrons to conduction band, $\Delta p = \Delta n$. However, in the presence of trap centers, Δp becomes

$$\Delta p = \Delta n + \Delta n_d, \quad (4)$$

where Δn_d is the density of electrons trapped at the defect sites. Equation (4) indicates that the defect level inside the bandgap plays an important role in the generation and recombination rates, which will be responsible for the NPC effect.

In order to illustrate this assumption, in Figures 2(b) and 2(c), we present a schematic representation of the transitions taking into account the trap level, indicated by ε_d . In Figure 2(b), without illumination, ε_d is partially filled electrons that are thermally excited from the valence band, represented by full symbols. The excess of holes (since it is a p -type sample) in the valence band and the electrons in conduction band are represented by open symbols and full symbols, respectively. Under illumination, represented in Figure 2(c), electrons are excited from valence band to conduction band leaving holes in the valence band (process 1). These holes diffuse in the valence band (process 2), and electrons from localized states in ε_d can recombine in valence band by reducing the number of holes in valence band (process 3). Eventually, electrons from conduction band can recombine at electron vacancies left in ε_d (process 4) by reducing the electron concentration in conduction band. In such scenario, processes 3 and 4 cause the reduction of carrier concentration in valence and conduction bands, leading to the decrease in the effective electrical conductivity under illumination giving rise to the observed NPC effect. However, this proposed model would be true only if the generation rates are not more effective than recombination rates (processes 3 and 4). Hence, the conditions $g_{dc} < r_{cd}$ and $g_{vd} < r_{dv}$ should be satisfied, where r_{dv} is the recombination from the level ε_d to the valence band, r_{cd} is the recombination from the conduction band to the level ε_d , g_{vd} is the generation rate from the valence band to the level ε_d , and g_{dc} is the generation rate from level ε_d to the conduction band. The generation and recombination rates can be derived according to the expressions¹⁸

$$r_{dv} = pn_d v S_p, \quad (5)$$

$$r_{cd} = n(N_d - n_d) v S_n, \quad (6)$$

$$g_{vd} = (N_d - n_d) N_v v S_p \exp\left(-\frac{E_g - \varepsilon_d}{k_B T}\right), \quad (7)$$

$$g_{dc} = n_d N_c v S_n \exp\left(-\frac{\varepsilon_d}{k_B T}\right), \quad (8)$$

where N_d is the density of defect centers, n_d is the density of states occupied by electrons, v is the thermal velocity of free carriers, S_p and S_n are the cross sections of holes and electrons, respectively, and N_c and N_v are the effective density of states in the conduction and valence band, respectively. We used $N_d \sim 10^{18} \text{ cm}^{-3}$, obtained from magnetoresistance measurements, i.e., we can extract N_d from the linear magnetoresistance present in this sample²³ and take $n_d = 0.5N_t$ as an average value. The cross sections values are $S_n = 10^{-20} \text{ cm}^2$, and $S_p = 30S_n$.¹⁸ In this case, we found that the energy ε_d is the same of ΔE .

Figure 3(a) presents g_{vd} and r_{dv} as a function of temperature. For $T > 170$ K, approximately, the condition $g_{vd} < r_{dv}$ is satisfied. This indicates that the NPC effect for such temperature region is mainly caused due to the reduction of holes in the valence band. Figure 3(b) shows g_{dc} and r_{cd} . According to this figure, the condition $g_{dc} < r_{cd}$ is satisfied only at $T < 170$ K, indicating that the reduction of electron in the conduction band is the main cause of the NPC effect for temperatures lower than 170 K.

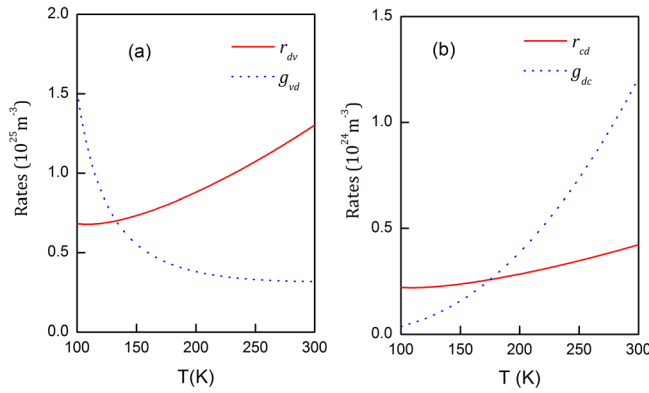


FIG. 3. (a) g_{vd} and r_{dv} as a function of temperature. For $T > 170$ K, approximately, the condition $g_{vd} < r_{dv}$ is satisfied. (b) g_{dc} and r_{cd} . The condition $g_{dc} < r_{cd}$ is satisfied only for $T < 170$ K indicating that the reduction of electron in the conduction band is the main cause of the NPC effect for temperatures lower than 170 K.

It is important to note that the configuration $g_{dc} > r_{cd}$ above 170 K (Figure 3(b)) should affect the total photoconductivity. In fact, in such configuration, we have a positive contribution to the photoconductivity since there is an increase in the electron density in the conduction band. On the other hand, in Figure 3(a), recombination from the defect level to the valence band dominates for $T > 170$ K, $r_{dv} > g_{vd}$, which gives a negative contribution (NPC) to photoconductivity at this temperature region. It is clear that, there is a competition between these two mechanisms. However, the rate of electrons recombined from the defect level to the valence band is higher than the rate of electrons generated in the conduction band. For instance, $g_{dc}(300K) \sim 1.2 \times 10^{24} m^{-3}$ while $r_{dv}(300) \sim 1.3 \times 10^{25} m^{-3}$. Hence, the contribution to the NPC effect is more effective for the total photoconductivity.

This model predicts that there is a transition temperature where the NPC effect contribution changes from the valence band to the conduction band. This temperature should be related to the position of the defect level inside the bandgap, which affects the amplitude of photoresponse as we discussed later. As temperature reduces, electrons became trapped at ε_d altering the recombination rates, which involve the transitions to the trap level. In this situation, even in dark conditions, the trapping of electrons at ε_d leads to increasing holes in the valence band. In fact, in Figure 4(a), one can observe a slight increase in the measured hole concentration in dark conditions (circle symbols). Under illumination, this effect still persists (square symbols). The temperature at which the thermal energy $k_B T$ corresponds to trapping level energy ($\varepsilon_d \sim 17.0$ meV) is around $T \sim 197$ K, i.e., below this temperature, the de-trapping occurs as the thermal energy becomes less effective. This temperature is in agreement with the temperature predicted by the model.

Figure 4(b) shows the values for which the NPC amplitude, σ_{min} , saturates for each temperature. According to this figure, σ_{min} presents a visible drop at some temperature below 200 K, indicating an enhancement of the NPC effect amplitude. Figure 4(c) presents the experimental hole mobility measured under light and dark conditions for temperatures in the range of 100–300 K. Apparently, from this figure, the illumination has no influence on the carrier mobility. However, it is

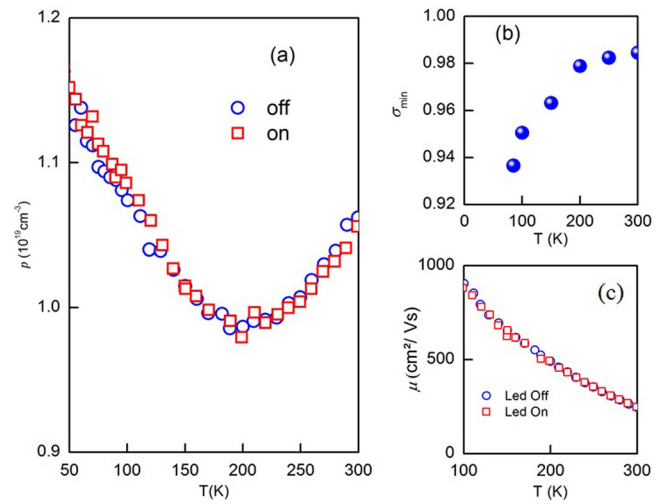


FIG. 4. (a) Hole concentration in dark conditions (open circles) and under illumination (square symbols). (b) Values for which the NPC amplitude, σ_{min} , saturates. σ_{min} presents a visible drop at some temperature below 200 K, indicating an enhancement of the NPC effect amplitude. (c) Experimental hole mobility measured under light and dark conditions for $T = 100$ –300 K. No visible variation with light is observed.

possible that the influence of light on carrier mobility is not detectable through this technique for this specific case. In fact, the NPC amplitude is only of a few percent as observed in Figure 1(a).

Finally, when illumination is removed, excited electrons from valence band stay trapped in the defect state, leading to a hole concentration in valence band higher than the initial concentration before the light is turned on. This explains the effect observed in the inset of Figure 1(a), where the final conductivity is higher than the original values for low temperatures.

In conclusion, we performed photoconductivity measurements using blue LED light in a p -type $Pb_{1-x}Sn_xTe$ film, for $x = 0.44$, and found that the sample exhibits NPC effect from $T \sim 85$ K up to room temperature. For a detailed analysis, additional measurements were performed under illumination and dark conditions, and transport properties and the energy of the trap levels were obtained. We found that the position of trap level in the gap influences the amplitude of the photoresponse, which indicates that this effect should be taken into account for future development of sensors device. Comparing the analysis of the experimental data to the calculated recombination rates, we found that the NPC effect is a consequence of the reduction of electrons and holes in the conduction and valence bands, respectively, due to the influence of the trap level in the dynamics of the recombination rates, which are also deeply temperature dependent. This verification, NPC transition from valence band to conduction band, gives a deeper comprehension of the behavior of generation and recombination process in this material.

In addition, the low noise level observed in the sample and the presence of NPC together with the persistent effect make $PbSnTe$ a potential basic material for the development of sensor devices and nonvolatile memories.

We would like to thank CAPES, CNPq, and FAPEMIG (APQ-00623-14) for financial support.

- ¹E. Abramof, S. O. Ferreira, P. H. O. Rappl, H. Closs, and I. N. Bandeira, *J. Appl. Phys.* **82**(5), 2405 (1997).
- ²I. U. Arachchige and M. G. Kanatzidis, *Nano Lett.* **9**(4), 1583 (2009).
- ³J. Liu, T. H. Hsieh, P. Wei, W. Duan, J. Moodera, and L. Fu, *Nat. Mater.* **13**, 178 (2014).
- ⁴J. O. Dimmock, I. Melngailis, and A. J. Strauss, *Phys. Rev. Lett.* **16**, 1193 (1966).
- ⁵P. Dziawa, B. J. Kowalski, K. Dybko, R. Buczko, A. Szczerbakow, M. Szot, E. Łusakowska, T. Balasubramanian, B. M. Wojek, M. H. Berntsen, O. Tjernberg, and T. Story, *Nat. Mater.* **11**, 1023 (2012).
- ⁶A. Martinez, F. Santiago, J. L. Davis, B. Houston, and H. D. Drew, *J. Appl. Phys.* **58**, 4618 (1985).
- ⁷D. Khokhlov, A. Galeeva, D. Dolzhenkoa, L. Ryabovaa, A. Nicoricib, S. Ganichevc, S. Danilovc, and V. Bel'kovc, *Proc. SPIE* **7453**, 74530J (2009).
- ⁸A. Berkeliev and K. Durdjev, *Sov. Phys. Semicond.* **5**, 646 (1971).
- ⁹B. A. Akimov, V. A. Bogoyavlenskii, L. I. Ryabova, and V. N. Vasilkov, *Phys. Rev. B* **61**, 16045 (2000).
- ¹⁰R. Sreekumar, R. Jayakrishnan, C. S. Kartha, and K. P. Vijaya-Kumar, *J. Appl. Phys.* **100**, 033707 (2006).
- ¹¹P. C. Wei, S. Chattopadhyay, M. D. Yang, S. C. Tong, J. L. Shen, C. Y. Lu, H. C. Shih, L. C. Chen, and K. H. Chen, *Phys. Rev. B* **81**, 045306 (2010).
- ¹²Y. Yang, X. Peng, H. S. Kim, T. Kim, S. Jeon, H. K. Kang, W. Choi, J. Song, Y. J. Doh, and D. Yu, *Nano Lett.* **15**(9), 5875 (2015).
- ¹³C. H. Lui, A. J. Frenzel, D. V. Pilon, Y.-H. Lee, X. Ling, G. M. Akselrod, J. Kong, and N. Gedik, *Phys. Rev. Lett.* **113**, 166801 (2014).
- ¹⁴R. B. Jacobs-Gedrim, M. Shanmugam, N. Jain, C. A. Durcan, M. T. Murphy, T. M. Murray, R. J. Matyi, R. L. Moor II, and B. Yu, *ACS Nano* **8**, 514 (2014).
- ¹⁵N. Gogurla, A. K. Sinha, D. Naskar, S. C. Kundub, and S. K. Ray, *Nanoscale* **8**, 7695 (2016).
- ¹⁶H. Nakanishi, K. J. M. Bishop, B. Kowalczyk, A. Nitzan, E. A. Weiss, K. V. Tretyakov, M. M. Apodaca, R. Klajn, J. F. Stoddart, and B. A. Grzybowski, *Nat. Lett.* **460**, 371 (2009).
- ¹⁷M. Nowak, K. Mistewicz, A. Nowrot, P. Szperlich, M. Jesionek, and A. Starczewska, *Sens. Actuators, A* **210**, 32 (2014).
- ¹⁸K. Lischka, R. Durstberger, G. Lindemann, and H. Stauding, *Phys. Status Solidi B* **123**, 319 (1984).
- ¹⁹S. de Castro, D. A. W. Soares, M. L. Peres, P. H. O. Rappl, and E. Abramof, *Appl. Phys. Lett.* **105**, 162105 (2014).
- ²⁰K. Lischka, *Phys. Status Solidi B* **133**, 17 (1986).
- ²¹P. H. O. Rappl, H. Closs, S. O. Ferreira, E. Abramof, C. Boschetti, P. Motisuke, A. Y. Ueta, and I. N. Bandeira, *J. Cryst. Growth* **191**, 466 (1998).
- ²²E. A. de Andrada e Silva, *Phys. Rev. B* **60**, 8859 (1999).
- ²³J. M. Schneider, M. L. Peres, S. Wiedmann, U. Zeitler, V. A. Chitta, E. Abramof, P. H. O. Rappl, S. de Castro, D. A. W. Soares, U. A. Mengui, and N. F. Oliveira, Jr., *Appl. Phys. Lett.* **105**, 162108 (2014).